RSC Advances

PAPER

View Article Online
View Journal | View Issue

Open Access Article. Published on 03 March 2017. Downloaded on 12/4/2025 11:40:37 AM.
This article is licensed under a Creative Commons Attribution 3.0 Unported Licence.

Cite this: *RSC Adv.*, 2017, 7, 14466

Preparation, characterization, and protein-resistance of films derived from a series of α-oligo(ethylene glycol)-ω-alkenes on H–Si(111) surfaces†

Guoting Qin,[c] Chi Ming Yam,[a] Amit Kumar,[a] J. Manuel Lopez-Romero,*[b] Sha Li,[a] Toan Huynh,[a] Yan Li,[a] Bin Yang,[a] Rafael Contreras-Caceres[b] and Chengzhi Cai*[a]

A series of oligo(ethylene glycol) (OEG)-terminated monolayers were prepared by photo-activated grafting of OEG-alkenes with the general formula $CH_2{=}CH(CH_2)_m(OCH_2CH_2)_nOCH_3$ (abbreviated as $C_{m+2}EG_n$, $m = 8, 9$; $n = 3–7$) on hydrogen-terminated silicon (111) surfaces using different deposition conditions. The films were characterized by contact-angle goniometry, ellipsometry, X-ray photoelectron spectroscopy (XPS) and tested for protein resistance. Films prepared under a higher vacuum showed a higher thickness and exhibited better protein resistance with increasing ethylene glycol (EG) units. Remarkably, the films prepared from $C_{10}EG_n$ were generally thicker than those from their corresponding homologues $C_{11}EG_n$, and displayed better resistance to protein adsorption, which were probably due to the odd–even effect from the alkyl chain. Prepared under high vacuum conditions (~10^{-5} mbar), the $C_{10}EG_7$ films with a thickness of 40 Å adsorbed <0.8% (the detection limit of N 1s XPS) monolayer of fibrinogen in a standard assay. The films remained protein-resistant (adsorbed <3% monolayer of fibrinogen) even after 28 days in phosphate buffered saline (PBS) at 37 °C or 17 days in MC3T3-E1 cell culture with 10% fetal bovine serum at 37 °C. Therefore, the $C_{10}EG_7$ films prepared under high vacuum conditions represent the most protein-resistant and stable films on non-oxidized silicon substrates.

Received 20th December 2016
Accepted 23rd February 2017

DOI: 10.1039/c6ra28497c

rsc.li/rsc-advances

Introduction

Modification of silicon surfaces with a stable, ultrathin and biocompatible monolayer is of great interest for the development of silicon-based miniature biodevices,[1] including field-effect transistors (FETs),[1–5] impedance and capacitance devices,[6–11] porous silicon photonic devices and probes,[12–14] drug carriers,[15] cantilever sensors,[16–18] and implantable devices, such as silicon-based neuron interfaces.[19–23] These silicon-based transducers interconvert specific biomolecular interactions/events with electrical/mechanical/optical signals of the silicon devices. One of the critical issues limiting the specificity and sensitivity of the transducers is the non-specific adsorption of proteins onto the silicon surfaces. Protein adsorption is also the first step of inflammatory and fibrotic responses leading to failure of many types of implanted devices.[24,25] The conventional way to address this issue is to utilize the SiO_2 layer on Si substrates and coat it with organosiloxane films terminated with poly- or oligo(ethylene glycol) (PEG or OEG).[26–31] However, the protein-resistance of such siloxane monolayers is not ideal; adsorption of 3–10% monolayer of proteins was reported.[31] The lower protein-resistance than the corresponding OEG-terminated alkanethiolate self-assembled monolayers (SAMs) on gold is likely due to the lower packing density and higher defect density of the siloxane films on silicon. Also, organosiloxane films are prone to hydrolysis in aqueous electrolytes, especially at basic conditions.[32,33] Furthermore, for electrical transducers, the sensitivity and signal to noise ratio are limited by the relatively thick oxide dielectric layer.[7,10] Although excellent protein-resistant properties have been demonstrated for zwitterions[34–36] and polypeptides[37] coatings, ultrathin films presenting OEG are still among the most widely used and the most protein-resistant coatings studied to date.[38–57] Moreover, we recently demonstrated that the high resistance to non-specific protein adsorption of OEG films allows the selective attachment of proteins onto the nanopatterns generated on such films by local oxidation using conductive atomic force microscopy (AFM).[58,59]

We and others have reported the photo-activated grafting of the α-OEG-ω-alkenes onto hydrogen-terminated silicon,

[a]Department of Chemistry & Center for Materials Chemistry, University of Houston, Houston, Texas 77204-5003, USA. E-mail: cai@uh.edu; Fax: +1-713-743-2709; Tel: +1-713-743-2710

[b]Departamento de Química Orgánica, Facultad de Ciencias, Universidad de Málaga, 29071 Málaga, Spain

[c]College of Optometry, University of Houston, Houston, TX 77204, USA

† Electronic supplementary information (ESI) available: Procedure of the synthesis of α-oligo(ethylene glycol)-ω-alkenes, calculation of thickness from ARXPS, and protein adsorption from ellipsometry. See DOI: 10.1039/c6ra28497c

 This journal is © The Royal Society of Chemistry 2017

Open Access Article. Published on 03 March 2017. Downloaded on 12/4/2025 11:40:37 AM.
This article is licensed under a Creative Commons Attribution 3.0 Unported Licence.

forming OEG-terminated monolayers that are directly bound to the silicon substrate *via* Si–C bonds (Scheme 1).[13,40,48,51,60–72] We performed this process in a simple apparatus combining a Schlenk tube with a quartz cell at a low vacuum level,[68,69,73,74] using OEG-terminated alkenes $C_{11}EG_n$ (n = 3, 6, 7 and 9). We found that $C_{11}EG_n$ with $n \geq 6$ led to films that reduced the adsorption of fibrinogen to ~3% monolayer after immersion in fibrinogen (1 mg mL^{-1}) for 1 h and brief washing with water.[68,69,73] The OEG films remained protein-resistant after 1 week in PBS (pH 7.4) at room temperature.[49] Notably, in the literature the protein-resistance of OEG-terminated films were often measured after washing the protein-treated samples with a detergent solution for a relatively long period of time.[75] Such a strong washing procedure resulted in a lower value of the protein adsorption compared to the procedure employed by us.[68,69,73] While the protein-resistance and stability of our previous OEG-terminated films on non-oxidized silicon were comparable to the reported OEG-terminated alkylthiolate monolayers on gold substrates,[76–78] further improvement is necessary for many applications stated above, such as implantable devices and biosensors.

The mechanism of protein resistance on OEG-terminated monolayers has been extensively studied theoretically and experimentally. It becomes clear that the packing density and the length of the OEG chains are the most important parameters. They directly affect the hydration of the OEG layer, which has been associated to the repulsion of proteins,[42,51,52,57,79–84] although the detailed mechanism awaits to be fully elucidated.[2a,28,53,60,78,80,85–92] In general, protein resistance increased with longer OEG chains especially at a low packing density. For alkanethiolate SAMs terminated with 3–6 EG units on Au(111) surfaces, the OEG chains adopt a helical conformation and amorphous state with a molecular cross-section of 21.3 $Å^2$. Their packing density is 21.4 $Å^2$ per molecule (equivalent to 4.7 molecules per nm^2).[45,51,78,80,81,91] The densities of previously reported alkyl terminated monolayers grown by hydrosilylation on Si are in the range of 0.45–0.55 alkyl chains per Si atom on a Si(111) surface (equivalent to 28.4–23.3 $Å^2$ per molecule),[66,71,93–95] which are lower than those of alkyl thiolate SAMs on gold due to the larger lattice parameters for Si(111). In our previous study, OEG monolayers on silicon substrate with low protein adsorption (<3% monolayer of fibrinogen)[69] had a packing density of 0.37–0.39 molecules per surface Si atom.

In addition to protein-resistance, film stability can also be greatly enhanced with dense and highly ordered hydrophobic alkyl layers that serve as a barrier against the penetration of oxygen and anion that induces oxidation at the silicon interface.[2a,96–98] Oligo(ethylene glycol) monolayers grafted directly onto silicon surfaces by silanization were shown to be unstable under either air or PBS solution conditions.[28] This instability was attributed to the oxidation at the silicon interface underneath the alkyl chains, which was susceptible to hydrolytic cleavage.[99] Lewis' group[100,101] functionalized Si(111) surfaces *via* Si–C bonds and achieved sterically bulky alkyl monolayers in a two-step process, involving Grignard reaction of the alkyl Grignard reagent with chlorine-terminated silicon surface. Unfortunately, high-purity Grignard reagents containing OEG chains are extremely difficult to prepare. Therefore, direct hydrosilylation of alkenes onto hydrogen-terminated silicon substrates is a more practical method. However, as mentioned above, the highest density of alkyl monolayers on silicon achieved to date *via* hydrosilylation is not comparable to that of alkanethiolated SAMs.[71] We expect that the presence of water and especially oxygen that has a high reactivity and diffusion rate, even at a low level in the system, may significantly decrease the film coverage due to the competition with the alkene for the surface active sites generated by the UV radiation.[71] Moreover, the resultant oxide defects accelerate the oxidation of adjacent silicon.[102] Therefore, decreasing oxygen level in the system is crucial to achieve a high packing density and low oxide defects. On the other hand, longer OEG chains generally increase protein resistance, but are expected to decrease packing density and stability of the films. In order to increase film stability, we aim to increase the packing density by optimizing the OEG length.

Herein, we report the study of monolayers derived from a series of α-OEG-ω-alkenes with the general formula of $CH_2{=}CH(CH_2)_m(OCH_2CH_2)_nOCH_3$ abbreviated as $\mathbf{C_{m+2}EG_n}$ (m = 8, 9; n = 3–7) on H–Si(111) surfaces. The study is focused on the effect of m with an odd (m = 9) or even (m = 8) number and n from 3 to 7 on the film thickness and protein resistance prepared at low (~1 mbar) and medium (~0.05 mbar) vacuum conditions (Scheme 1). Contact angle goniometry, ellipsometry and XPS were used to characterize and investigate the protein resistance of OEG films. We further improved the deposition vacuum to the level of 10^{-5} mbar, resulting in monolayers with a thickness of 40 Å. These monolayers represent the most protein resistant and stable monolayers on non-oxidized silicon reported to date.[28,75]

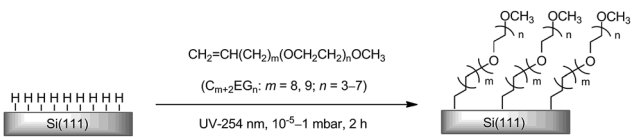

Scheme 1 Photo-induced surface hydrosilylation of OEG-terminated alkene monolayers on silicon surfaces.

Materials and methods

Materials

Commercial chemicals, including sulfuric acid (Sigma-Aldrich), 30% hydrogen peroxide solution (Sigma-Aldrich), 40% ammonium fluoride solution (Sigma-Aldrich), dichloromethane (Sigma-Aldrich), petroleum ether (Sigma-Aldrich), absolute ethanol (Alfa Aesar), and 10% buffer-HF (Transene) were used without purification. Fibrinogen, minimum essential medium alpha modification (αMEM) and Dulbecco's modified eagle's medium (DMEM) were purchased from Sigma Aldrich. Silicon (111) wafers were purchased from Silicon Quest Int'l. Inc. The synthesis of α-OEG-ω-alkenes with the general formula of $CH_2{=}CH(CH_2)_m(OCH_2CH_2)_nOCH_3$ ($\mathbf{C_{m+2}EG_n}$, m = 8, 9; n = 3–7) are described in ESI.† OEGs where prepared under N_2

Open Access Article. Published on 03 March 2017. Downloaded on 12/4/2025 11:40:37 AM.
This article is licensed under a Creative Commons Attribution 3.0 Unported Licence.

atmosphere and stored at 5 °C in amber vials under Ar to prevent the presence of water and O_2. MC3T3-E1 fibroblast cells and osteoblast D1 cells were provided from Dr David Mooney at Harvard University.

Preparation of H–Si(111) substrates

Single side polished silicon (111) wafer (boron-doped, P-type, 1–10 Ω cm resistivity, miscut angle of ±0.5°) was cut into pieces of 1 × 1 cm^2, cleaned with Piranha solution (concentrated H_2SO_4/30% H_2O_2, 3 : 1 v/v) for 10 min at ∼80 °C to remove organic contaminates. **Caution**: Piranha solutions react violently with organic materials and should be handled with extreme care. The freshly cleaned sample was immersed in an Ar-saturated, 40% NH_4F solution (prepared by gently bubbling the solution with argon for 10 minutes prior to use) for 20 min followed by rinse with argon-saturated Millipore water and dried with a stream of argon.

Photo-activated grafting

Previous apparatus. We initially used a simple setup combining a Schlenk tube with a quartz cell for photo-induced surface hydrosilylation on hydrogen-terminated silicon substrates with alkene as described in our previous publications.[68,69,103] The hydrosilylation was carried out at low (∼1 mbar) and medium vacuum (∼0.05 mbar) conditions, respectively, under illumination with a hand-hold 254 nm UV-lamp (Model UVLS-28, UVP) for 2 h, followed by washing sequentially with petroleum ether, ethanol, and CH_2Cl_2, and finally drying with a stream of Ar.[104]

Improved apparatus with a high vacuum for the preparation of high quality $C_{10}EG_7$ films. The apparatus consists of a glass chamber sealed with a quartz plate (5 cm in diameter) *via* a Viton o-ring (Fig. 1). The chamber is connected to a liquid nitrogen cold-trap and an oil diffusion pump with the ultimate vacuum of 10^{-6} mbar. A linear manipulator is used to translate the sample. To reduce contamination, the sample is attached onto a freshly cleaved surface of a piece of mica that is glued onto a steel disk. To enhance the adhesion between the mica and the backside of the sample, a tiny droplet of the alkene is applied on the mica. The steel disk is then attached onto the magnetic disk at the end of the manipulator. A droplet of the alkene is placed on top of the quartz plate, and the plate is immediately attached to the apparatus and sealed with a Viton o-ring. After the vacuum reaches 10^{-5} mbar, the substrate is brought down to allow contact with the alkene droplet, thus forming a thin layer of the alkene sandwiched between the quartz plate and the H–Si surface. The substrate is then subjected to UV irradiation with a handheld 254 nm UV lamp for 2 h followed by washing sequentially with petroleum ether, ethanol, and CH_2Cl_2, and finally drying with a stream of Ar.

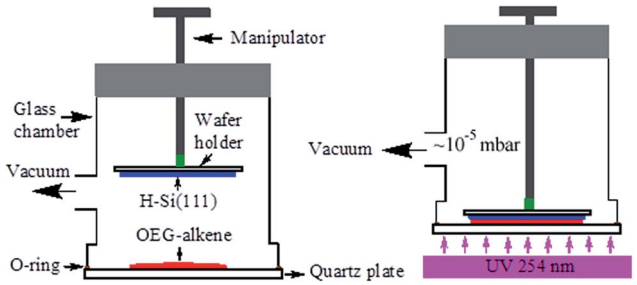

Fig. 1 Improved apparatus for preparation of OEG films *via* photo-activated hydrosilylation.

Contact-angle goniometry

Water drops were dispersed onto the film surfaces using a micro-Electrapette 25 (Matrix Technologies). Advancing and receding contact angles ($\theta_{a/r}$) were measured using a goniometer (Rame-Hart, model 100). The pipette tip was kept in contact with the drop during the measurements. At least four drops of probe liquid were measured for each sample, and the mean values were reproducible within ±1°.

Ellipsometry

An ellipsometer (Rudolph Research, Auto EL III), operated with a 632.8 nm He–Ne laser at an incident angle of 70°, was employed for thickness measurement. A refractive index of 1.45 was assumed for the prepared films. At least four measurements were taken for each sample, and the mean values were reproducible within ±1 Å.

X-ray photoelectron spectroscopy (XPS)

A PHI 5700 X-ray photoelectron spectrometer, equipped with a monochromatic Al Kα X-ray source ($h\nu$ = 1486.7 eV) at a take-off angle (TOA) of 45° from the film surface was employed for XPS measurement. High-resolution XPS spectra were obtained by applying a window pass energy of 23.5 eV and the following numbers of scans: Si 2p, 5 scans; C 1s, 20 scans; O 1s, 10 scans; N 1s, 20–40 scans. The binding energy scales were referenced to the Si 2p peak at 99.0 eV. XPS spectra were curve fitted and the intensities measured as peak areas were calculated using Phi Multipak V5.0A from Physical Electronics.

Protein resistance

The fibrinogen solution was prepared by dissolving 1 mg fibrinogen (Sigma) in 1 mL of PBS (consisting of 0.01 M phosphate and 0.14 M NaCl, pH 7.4, Sigma) in a vial. The test samples were immersed in the fibrinogen solution at 20–25 °C for 1 h. The samples were then washed under a gentle flow of Millipore water for about 15 seconds, dried with a flow of Ar, and subjected to contact angle, ellipsometric and XPS measurements.

In addition to the fibrinogen adsorption experiment above, the protein-resistance of the OEG monolayers on silicon was also evaluated in culture of αMEM for MC3T3-E1 cells and DMEM for D1 cells. In these experiments, the test samples were incubated in cell culture media with or without live cells over a specific period of time. It should be noted that the culture media in all cases contained 10% fetal bovine serum (FBS) that consists of a wide variety of proteins necessary for the cultured cells to survive, grow and divide.

Open Access Article. Published on 03 March 2017. Downloaded on 12/4/2025 11:40:37 AM.
This article is licensed under a Creative Commons Attribution 3.0 Unported Licence.

Long-term stability of $C_{10}EG_7$ films prepared under high vacuum

The stability of the $\mathbf{C_{10}EG_7}$ films on silicon substrates was evaluated by incubating the samples in PBS at 37 °C for 28 days followed by the fibrinogen adsorption experiment, or in MC3T3 cell culture in αMEM with 10% fetal bovine serum at 37 °C for 17 days. The amount of adsorbed proteins was measured by the increase of ellipsometric thickness. The optimized films $\mathbf{C_{10}EG_7}$ films were also measured by N 1s XPS using fibrinogen monolayer adsorbed on H–Si(111) as a standard (see below).

Amount of protein adsorbed on the $C_{10}EG_7$ films

In addition to ellipsometric measurement, the amount of proteins adsorbed onto the $\mathbf{C_{10}EG_7}$ films prepared under high vacuum was also quantified by N 1s XPS and expressed as percentage of a fibrinogen monolayer (% ML) calculated using eqn (1):

$$\text{Adsorbed protein (\% ML)} = 100 \times N_{(\text{OEG})}/N_{(\text{H–Si})} \quad (1)$$

where $N_{(\text{OEG})}$ is the intensity of N 1s signal from the protein adsorbed on the $\mathbf{C_{10}EG_7}$ monolayer, and $N_{(\text{H–Si})}$ is the intensity of N 1s signal from a monolayer (6 nm thick) of fibrinogen adsorbed on a H–Si(111) substrate. It should be noted that eqn (1) only gives an estimation of the amount of adsorbed proteins using a monolayer of fibrinogen as the standard because the amount of adsorbed fibrinogen might be overestimated by ignoring the higher attenuation of the N signals from the monolayer of fibrinogen on H–Si surfaces. Lower accuracy is expected for estimating the amount of proteins adsorbed onto surfaces immersed in cell culture media using eqn (1) because the system contains many different proteins with varied nitrogen compositions. Despite the limitations, the XPS method (detection limit: ~0.8% ML) is more sensitive than ellipsometric thickness measurement.

Results and discussion

$C_{10}EG_n$ films on Si(111) prepared under low vacuum

We carried out the photo-induced surface hydrosilylation of H–Si(111) substrates with a series of OEG-alkenes ($\mathbf{C_{10}EG_n}$) using the setup described elsewhere.[69] Table 1 summarizes the advancing and receding contact angles of water ($\theta_{a/r}$) and ellipsometric thicknesses (T_e) for the $\mathbf{C_{10}EG_n}$ films on Si(111) surfaces upon exposure to UV-254 nm irradiation under ~1 mbar for 2 h. The advancing water contact angle θ_a and ellipsometric thickness T_e of the $\mathbf{C_{10}EG_n}$ films on Si(111) surfaces decreased from 59 to 51° and increased from 21 to 28 Å, respectively, with an increase of EG units from three to seven. These contact angle values are consistent with those reported for other OEG-terminated alkene films prepared under similar conditions on Si(111) surfaces.[68,69] The low hysteresis ($\Delta\theta = 2$–3°) for the films indicates smooth and homogeneous surfaces. As shown in Table 2, XPS data for the $\mathbf{C_{10}EG_n}$ films on Si(111) surfaces show two C 1s peaks and one O 1s peak. For the carbon peaks, the one at higher binding energy (~287 eV) is assigned to the carbon atoms that are adjacent to an oxygen atom, and the one at lower binding energy (~285 eV) is assigned to the rest of the carbon atoms.[43,69,80,105] The ratios of the integrated areas of the deconvoluted C 1s signals from these two types of carbon atoms, ($C_{C–C}/C_{C–O}$), are close to the stoichiometric ratio. The peak at 533 eV is assigned to the oxygen atoms of the EG units.

Based on the data above, calculated packing densities of the films derived from $\mathbf{C_{10}EG_n}$ ($n = 3, 6$) were similar to those we previously reported.[69] These data are summarized in Table S1 in the ESI.† As expected, the packing density, represented as A_m (unit surface area per grafted molecule) and $N_{chains}/N_{surf,Si}$ (number of hydrocarbon chains per surface silicon atom), decreases with increasing OEG monolayer length grafted on the silicon substrate. It should be noted, however, that the measured ellipsometric thickness may represent an overestimate due to the adsorption of water to the OEG-terminated films. Indeed, recent studies[106–108] indicated the presence of tightly bound water on top of organic thin films, even those presenting hydrophobic alkynyl groups, which could not be removed by ultrahigh vacuum.

After immersing the $\mathbf{C_{10}EG_n}$-coated Si(111) substrates with a fibrinogen solution for 1 h, both T_e and $\theta_{a/r}$ indicate that the films of $\mathbf{C_{10}EG_3}$, $\mathbf{C_{10}EG_4}$, and $\mathbf{C_{10}EG_5}$ prepared on Si(111) surfaces readily adsorbed the protein, as shown by an increase of both of T_e (14, 9, and 4 Å, respectively) and θ_a (7, 7, and 4°, respectively), while very low protein adsorption was found on

Table 1 Advancing and receding contact angles of water ($\theta_{a/r}$) and ellipsometric thicknesses (T_e) for $C_{10}EG_n$ films on Si(111) prepared at low vacuum (~1 mbar) and medium vacuum (~0.05 mbar) conditions before and after treatment with fibrinogen

	Low vacuum (~1 mbar)				Medium vacuum (~0.05 mbar)			
	Before treatment with fibrinogen		After treatment with fibrinogen		Before treatment with fibrinogen		After treatment with fibrinogen	
Film	$\theta_{a/r}$,[a] deg	T_e,[b] °C	$\theta_{a/r}$,[a] deg	T'_e,[b] °C	$\theta_{a/r}$,[a] deg	T_e,[b] °C	$\theta_{a/r}$,[a] deg	T'_e,[b] °C
$\mathbf{C_{10}EG_3}$	59/56	21	66/49	35				
$\mathbf{C_{10}EG_4}$	56/54	22	63/41	31	55/52	30	56/53	32
$\mathbf{C_{10}EG_5}$	55/53	25	59/47	29	52/50	33	52/50	35
$\mathbf{C_{10}EG_6}$	53/51	27	55/52	29	52/49	34	53/50	35
$\mathbf{C_{10}EG_7}$	51/49	28	52/49	29	50/47	36	50/47	36

[a] Standard deviation of measurements were ±1°. [b] Standard deviation of measurements were ±1 Å.

Open Access Article. Published on 03 March 2017. Downloaded on 12/4/2025 11:40:37 AM.
This article is licensed under a Creative Commons Attribution 3.0 Unported Licence.

Table 2 XPS data for $C_{10}EG_n$ films on Si(111) prepared at low vacuum conditions

	XPS			
			$[C_{C-C}]/[C_{C-O}]$	
Film	C 1s	O 1s	Expected	Measured
$\mathbf{C_{10}EG_3}$	284.8, 286.7	533.0	1 : 0.9	1 : 0.9
$\mathbf{C_{10}EG_4}$	284.9, 286.6	532.9	1 : 1.1	1 : 1.1
$\mathbf{C_{10}EG_5}$	284.8, 286.7	532.9	1 : 1.3	1 : 1.4
$\mathbf{C_{10}EG_6}$	284.8, 286.7	532.9	1 : 1.6	1 : 1.6
$\mathbf{C_{10}EG_7}$	284.8, 286.6	533.0	1 : 1.8	1 : 1.9

the $\mathbf{C_{10}EG_6}$- and $\mathbf{C_{10}EG_7}$-coated surfaces, as indicated by the nearly unchanged $\theta_{a/r}$ and T_e values (Tables 1 and S1†). For comparison, a freshly prepared H–Si(111) substrate was also subjected to protein treatment for 1 h. As expected, fibrinogen readily adsorbed on the hydrophobic H–Si(111) surface, resulting in a film with $T_e = \sim 60$ Å and $\theta_{a/r} = \sim 80°/<20°$, corresponding to a monolayer of fibrinogen.[69] Thus, by ellipsometric measurement, the degree of protein adsorption on the $\mathbf{C_{10}EG_n}$-coated surfaces decreased from ~23% to ~2% monolayer of fibrinogen with an increase of EG units from three to seven (Fig. 2). Therefore, with at least six EG units, the OEG-terminated films derived from the $\mathbf{C_{10}EG_n}$ series on Si(111) surfaces and prepared at low vacuum conditions (~1 mbar) effectively resisted the protein adsorption, which was comparable to those films derived from OEG-terminated thiolates on Au(111) surfaces that also displayed increasing protein resistance with longer EG chain length.[49,53,57,78]

$C_{10}EG_n$ films on Si(111) prepared at medium vacuum conditions

In order to reduce the presence of water and specially oxygen which compete with the alkene for the surface active sites generated by UV, we prepared the $\mathbf{C_{10}EG_n}$ films on Si(111) surfaces under an improved vacuum (~0.05 mbar, termed as medium vacuum). Under such a vacuum, the $\mathbf{C_{10}EG_3}$ films could not be prepared since the adsorbate $\mathbf{C_{10}EG_3}$ readily evaporated. Table 1 summaries $\theta_{a/r}$ and T_e of the $\mathbf{C_{10}EG_n}$ films on Si(111) surfaces upon exposure to 254 nm UV irradiation under ~0.05 mbar for 2 h. θ_a and T_e of the $\mathbf{C_{10}EG_n}$ films on Si(111) surfaces decreased from 55 to 50° and increased from 30 to 36 Å, respectively, with an increase of n from 4 to 7. There was a significant increase of T_e by ~8 Å for the $\mathbf{C_{10}EG_n}$ films with the same number of EG units on Si(111) surfaces as the pressure of the system was reduced from ~1 to ~0.05 mbar. A low hysteresis ($\Delta\theta = 2$–$3°$) was still observed for the films.

After treatment of the $\mathbf{C_{10}EG_n}$-coated Si(111) substrates with a fibrinogen solution for 1 h, only a low level of protein adsorption on the $\mathbf{EG_3}$-, $\mathbf{EG_4}$-, $\mathbf{EG_5}$- and $\mathbf{EG_6}$-terminated films was observed, as indicated by the small changes of $\theta_{a/r}$ (≤2°) and T_e (≤2 Å) values (Tables 1, S1† and Fig. 2). The increase of 2 Å in thickness represents an adsorption of ~3% monolayer of fibrinogen (60 Å thick for a monolayer). No protein adsorption on the $\mathbf{C_{10}EG_7}$ films could be detected by water contact angle and ellipsometry.

Notably, the thicknesses of the $\mathbf{C_{10}EG_n}$ films are almost equal to the theoretical molecular length of the compounds, assuming the molecules adopt a zig-zag 'all-trans' conformation.[80] However, the maximum packing density of long alkyl chains grafted on H–Si(111) by surface hydrosilylation is only ~0.55 alkyl chains/surface Si atom,[66] corresponding to a density of 23.3 Å^2 per molecule. Hence, in our case it is highly unlikely that the packing density reaches the theoretical value of 19.1 Å^2 per molecule when adopting a zig-zag conformation.[80] Furthermore, the improved protein resistance (Fig. 2) indicates that the OEG chains most likely are in an amorphous state. Also, XPS did not show the presence of silicon oxide underneath the film. Therefore, the high thickness can be attributed to the growth of a partial second layer due to the presence of radicals on the film. There might be three likely pathways to generate radicals from monolayers:[109] (1) direct photodissociation of C–H or C–C bonds *via* vacuum ultraviolet (VUV); (2) photoelectron mediated dissociation of monolayer; (3) reactive oxyspecies generated by UV light, such as singlet oxygen and hydroxyl radicals. The UV induced generation of reactive oxy species is possible[109,110] although the oxygen level in our vacuum system was 1.5×10^4 times lower than that in air. Also, the radicals could be generated *via* the cleavage of the C–H bonds on the CH_3 headgroup of the monolayers by the very minor amount of 185 nm UV light, since the C_{C-C}/C_{C-O} ratios match those of the molecules (Tables 2 and 5).

We then investigated the thickness of $\mathbf{C_{10}EG_7}$ films prepared from hydrosilylation at different exposure time under UV. The film thickness was monitored by ellipsometry, and was also validated by angle-resolved XPS (Fig. 3). It can be seen that the film thickness rapidly increased under UV light before it slowed down at around 2 h, during which the formation of the first layer was probably the dominating factor of the thickness growth. After that, the growth of a second layer may account for the increasing thickness, although it was much slower than that of the first layer. Interestingly, the surface hydrophilicity and homogeneity seem to be constant regardless of the UV

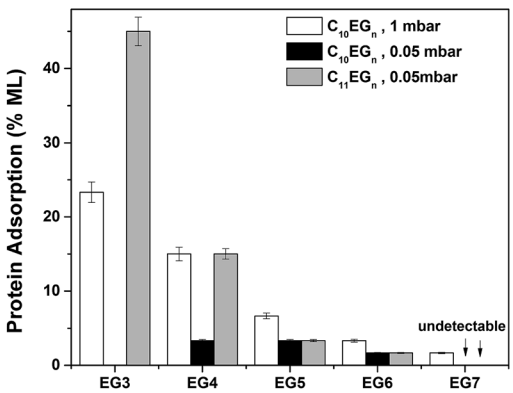

Fig. 2 Adsorption of fibrinogen (% monolayer) estimated by the increase of ellipsometric thickness upon fibrinogen treatment of the $C_{10}EG_n$ and $C_{11}EG_n$ films on Si(111) prepared at low vacuum (~1 mbar) and medium vacuum (~0.05 mbar) conditions. The errors are derived from the errors of ellipsometric measurements.

Open Access Article. Published on 03 March 2017. Downloaded on 12/4/2025 11:40:37 AM.
This article is licensed under a Creative Commons Attribution 3.0 Unported Licence.

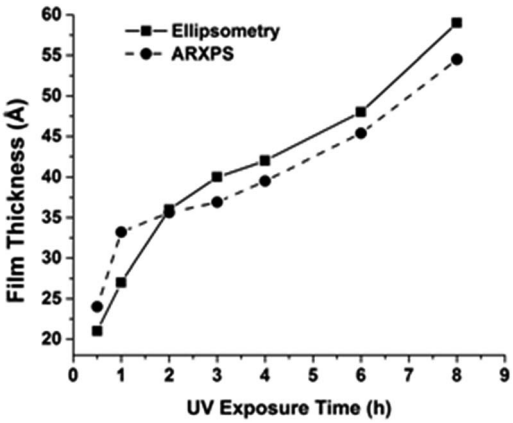

Fig. 3 Thickness of $C_{10}EG_7$ films prepared under medium vacuum condition at different UV exposure time. One sample was prepared at each time point.

exposure time, as can bee seen from the water contact angle data (Table 3).

C11EGn films on Si(111) prepared at medium vacuum conditions

OEG-terminated films derived from $\mathbf{C_{11}EG_n}$ (n = 3, 6, 7, 9) on Si(111) under low vacuum conditions were described in our previously reports.[68,69] The films with three EG units adsorbed 30–60% monolayer of fibrinogen, while the films with more than six EG units reduced the adsorption of fibrinogen to ~3% monolayer. We expected that both the packing density and the protein resistance of the $\mathbf{C_{11}EG_n}$ films on Si(111) surfaces would be improved under higher vacuum conditions (~0.05 mbar).

Table 3 Advancing and receding contact angles of water ($\theta_{a/r}$) for $C_{10}EG_n$ films on Si(111) prepared at medium vacuum and different UV exposure time

Exposure time, h	0.5	1	2	3	4	6	8
$\theta_{a/r}$,[a] deg	51/48	50/47	50/47	50/48	51/48	51/47	53/50

[a] Standard deviation of measurements were ±1°.

Table 4 Advancing and receding contact angles of water ($\theta_{a/r}$), ellipsometric thicknesses (T_e) for $C_{11}EG_n$ films on Si(111) prepared at medium vacuum conditions (~0.05 mbar) before and after treatment with fibrinogen

	Before protein adsorption		After protein adsorption	
Film	$\theta_{a/r}$,[a] deg	T_e,[b] Å	$\theta_{a/r}$,[a] deg	T_e,[b] Å
$\mathbf{C_{11}EG_3}$	61/59	25	75/<20	52
$\mathbf{C_{11}EG_4}$	57/55	28	63/47	37
$\mathbf{C_{11}EG_5}$	52/49	30	53/50	32
$\mathbf{C_{11}EG_6}$	51/48	32	52/49	33
$\mathbf{C_{11}EG_7}$	50/47	34	50/47	34

[a] Standard deviation of measurements were ±1°. [b] Standard deviation of measurements were ±1 Å.

Table 4 summaries θ_a/θ_r and T_e for the $\mathbf{C_{11}EG_n}$ films on Si(111) surfaces upon exposure to UV-254 nm irradiation under ~0.05 mbar for 2 h. The advancing water contact angle θ_a and ellipsometric thickness T_e of the $\mathbf{C_{11}EG_n}$ films decreased from 61 to 50° and increased from 25 to 34 Å, respectively, with the increase of OEG chain length (n) from 3 to 7. Indeed, there was a ~5 Å increase of T_e for the $\mathbf{C_{11}EG_n}$ films with the same number of EG units on Si(111) surfaces as the pressure of the system was reduced from ~1 to ~0.05 mbar. A low hysteresis ($\Delta\theta$ = 2–3°) was still observed for the films. The XPS data for the $\mathbf{C_{11}EG_n}$ films on Si(111) surfaces (Table 5) show two C 1s peaks at ~285 and ~287 eV, respectively, and one O 1s peak at ~533 eV, similar to those for the $\mathbf{C_{10}EG_n}$ films described in the previous section. The (C_{C-C}/C_{C-O}) ratios are also in good agreement with the expected ratios.

After treatment of the $\mathbf{C_{11}EG_n}$-coated Si(111) substrates with a fibrinogen solution for 1 h, both T_e and $\theta_{a/r}$ indicate that the films of $\mathbf{C_{11}EG_3}$ and $\mathbf{C_{11}EG_4}$ prepared on Si(111) surfaces readily adsorbed the protein, as shown by both an increase of θ_a (14 and 6°, respectively) and T_e (27 and 9 Å, respectively). The estimated fibrinogen adsorption based on the ellipsometric data is presented in Fig. 2 and Table S1,† showing a decrease of fibrinogen adsorption from ~45% to ~3% monolayer with increasing EG units from three to six, and the fibrinogen adsorption on the $\mathbf{C_{11}EG_7}$ films was not detectable.

$C_{10}EG_n$ *vs.* $C_{11}EG_n$ films – thickness and packing

Since the methylene chain of the OEG films is *ca.* 1–2 Å per unit (–CH_2–), the $\mathbf{C_{11}EG_n}$ films are expected to be 1–2 Å thicker than the $\mathbf{C_{10}EG_n}$ films with the same number of EG units. However, T_e of the $\mathbf{C_{11}EG_n}$ films was smaller than that of the $\mathbf{C_{10}EG_n}$ films by ~2 Å (Fig. 4). As shown above, for the $\mathbf{C_{10}EG_n}$ films, an increase of one EG unit led to an increase of 1–3 Å of the film thickness. However, an increase of one carbon atom in the alkyl chain with the same EG units showed, surprisingly, a decrease of ~2 Å. Additionally, the calculated packing densities decreased with the increasing number of EG units from 3 to 7 for both $\mathbf{C_{10}EG_n}$ and $\mathbf{C_{11}EG_n}$ films as shown in Table S1.† To rationalize this intriguing result, we note that there is probably an 'Odd–Even' effect from the alkyl chain as discussed below using a simplified packing model. The 'Odd–Even' effect often affects the packing density and wettability of SAMs, such as n-carboxylic acids and alkylthiolates, on various substrates,

Table 5 XPS data for $C_{11}EG_n$ films on Si(111) prepared at medium vacuum conditions

	XPS			
			$[C_{C-C}]/[C_{C-O}]$	
Film	C 1s	O 1s	Expected	Measured
$\mathbf{C_{11}EG_3}$	284.7, 286.5	533.0	1 : 0.8	1 : 0.7
$\mathbf{C_{11}EG_4}$	284.8, 286.6	533.0	1 : 1.0	1 : 1.1
$\mathbf{C_{11}EG_5}$	284.8, 286.6	533.0	1 : 1.2	1 : 1.1
$\mathbf{C_{11}EG_6}$	284.8, 286.6	533.0	1 : 1.4	1 : 1.3
$\mathbf{C_{11}EG_7}$	284.6, 286.4	533.0	1 : 1.6	1 : 1.7

Open Access Article. Published on 03 March 2017. Downloaded on 12/4/2025 11:40:37 AM.
This article is licensed under a Creative Commons Attribution 3.0 Unported Licence.

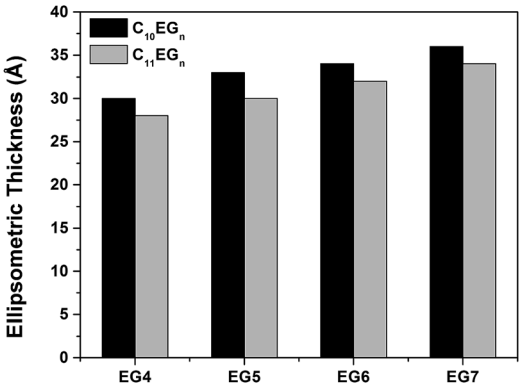

Fig. 4 Ellipsometric thicknesses (Å) of $C_{10}EG_n$ and $C_{11}EG_n$ films on Si(111) prepared at medium vacuum conditions.

such as graphite, Au(111), and Ag(111).[111,112] However, to our knowledge, no study has been reported on the possible odd–even effect on OEG-terminated alkyl monolayers on silicon. Confirming this effect for our systems requires systematic study of the OEG-terminated films with a series of alkyl chain length, which is out of the scope for the current study.

To account for the above observed higher packing density of the $\mathbf{C_{10}EG_n}$ films over the corresponding $\mathbf{C_{11}EG_n}$ films, we use an idealized packing model shown in Fig. 5. The lone-pair electrons of the bottom oxygen atoms (O–C(11)) in the $\mathbf{C_{11}EG_n}$ films, which has an odd number of carbon atoms in the alkyl chain, interact with the $\mathbf{H_2}$C(11) moieties in the adjacent *alkyl* chains. In comparison, the bottom O atoms (O–C(10)) in the $\mathbf{C_{10}EG_n}$ films, which has an even number of carbon atoms in the alkyl chain, interact with the $\mathbf{H_2}$C(11) moieties in the adjacent *ethylene oxide* chains that are more electronegative than the *alkyl* chains in the above case. Therefore, the bottom oxygen atoms have a more favorable interaction with the methylene moieties in the $\mathbf{C_{10}EG_n}$ films than the $\mathbf{C_{11}EG_n}$ films, leading to higher packing density in the former. To a lesser extent, the top oxygen atoms may prefer to interact with the adjacent ethylene oxide moieties in the $\mathbf{C_{10}EG_n}$ films than with the methyl groups in the $\mathbf{C_{11}EG_n}$ films.

$C_{10}EG_7$ films grown with improved apparatus under high vacuum conditions

Despite of the simplicity of our previous apparatus for photo-activated grafting, it has several limitations. First, due to the close proximity of the H–Si(111) substrate to the alkene droplet placed in the small quartz cell,[68,69] the Si–H surface is easily contaminated during the degassing process by the volatile reactive impurities such as H_2O and O_2. Second, the size (<1 cm^2) of the silicon sample was limited by the size of the available quartz cells. Third, the manipulation of the sample was difficult to master, and flipping of the samples often occurred. To address these drawbacks, we designed the second-generation apparatus for photo-activated grafting of thin films (Fig. 1). The new apparatus has the following improvements. First, during the degassing step, the H–Si substrate surface is located above the outlet to the vacuum and is far away from the alkene droplet, thus reducing the possibility of contamination. Second, only the quartz window needs to be cleaned before each use. Finally, the apparatus is easy to use, and can handle larger samples (up to 2×2 cm^2). Most importantly, the vacuum was improved from 0.05 mbar to 10^{-5} mbar. On the basis of the above results, we expected that the improvement of the vacuum conditions would greatly increase the packing density of the OEG-terminated films and thus enhance the protein-resistance and long-term stability of the films. The above study identified $\mathbf{C_{10}EG_7}$ as the best adsorbate, also because we observed substantial evaporation of EG_n-alkenes with $n < 6$ during deposition under such a high vacuum condition, resulting in poor quality film. Therefore, we focused on the study of the $\mathbf{C_{10}EG_7}$ films prepared using the new apparatus under high vacuum (10^{-5} mbar).

The resultant $\mathbf{C_{10}EG_7}$ films on silicon (111) were characterized by contact angle goniometry, ellipsometry, and AFM. As shown in Fig. 6, the AFM contact mode image of a $\mathbf{C_{10}EG_7}$ film revealed the underlying atomic steps of the silicon substrate, indicating that the film was ultraflat. The advancing and receding water contact angles were 51°/49° with a low hysteresis $\Delta\theta = 2°$, also indicating a homogeneous surface. The ellipsometric thickness of the film was increased from 36 Å to 40 ± 1 Å, reaches the molecular length of $\mathbf{C_{10}EG_7}$ (38.7 Å). This ellipsometric thickness was in agreement with the thickness of 39.5 Å measured by variable angle XPS (see ESI, Fig. S2†). These results

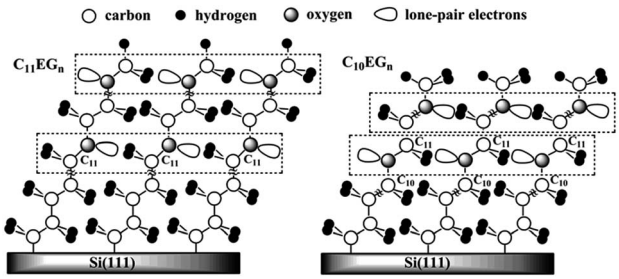

Fig. 5 Schematic representations of $C_{11}EG_n$ (odd-numbered) and $C_{10}EG_n$ (even-numbered) films on Si(111).

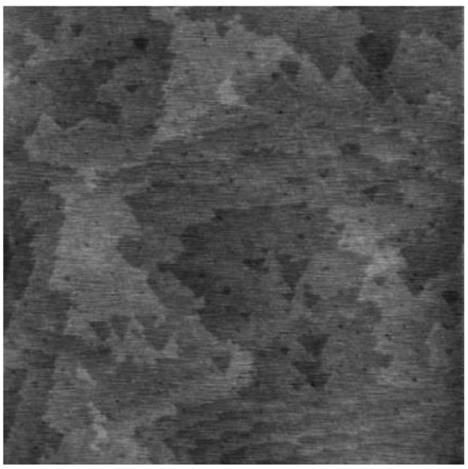

Fig. 6 An AFM contact mode image (1×1 μm^2, 5 nm contrast) of $C_{10}EG_7$ monolayer on Si(111).

Open Access Article. Published on 03 March 2017. Downloaded on 12/4/2025 11:40:37 AM.
This article is licensed under a Creative Commons Attribution 3.0 Unported Licence.

indicated that the molecules on the surfaces were densely packed.

Protein resistance and stability of the $C_{10}EG_7$ films prepared under high vacuum conditions

The stability of the films on silicon substrates was evaluated by incubation of the samples in PBS or cell culture media at 37 °C for the specified period of time, followed by the fibrinogen adsorption experiment. The amount of the adsorbed proteins was determined by the N 1s signal from XPS using eqn (1). As shown by the N 1s region of the XPS spectrum in Fig. 7, freshly prepared $\mathbf{C_{10}EG_7}$ films did not adsorb protein to the detection limit of N 1s XPS (0.8% monolayer of fibrinogen). Even after storage for 14 d under ambient conditions or 28 d in PBS (pH 7.4) at 37 °C, the $\mathbf{C_{10}EG_7}$ coated silicon surfaces remained protein resistant, with no N 1s signal was detected after the fibrinogen adsorption experiment. Furthermore, the protein-resistance and stability of the $\mathbf{C_{10}EG_7}$ films on silicon was tested with cell culture media (αMEM for MC3T3-E1 cells and DMEM for D1 cells) and cell cultures with 10% fetal bovine serum (FBS), which contained a rich variety of proteins. As shown in Fig. 8, the amount of protein adsorbed onto the $\mathbf{C_{10}EG_7}$ surfaces were 2.0% ± 0.8% ML after 12 d in αMEM with 10% FBS, 2.8% ± 0.8% ML after 17 d in MC3T3-E1 cell culture, 1.4% ± 0.8% ML after 5 d in DMEM with 10% FBS, and 1.2% ± 0.8% ML after 7 d in D1 cell culture.

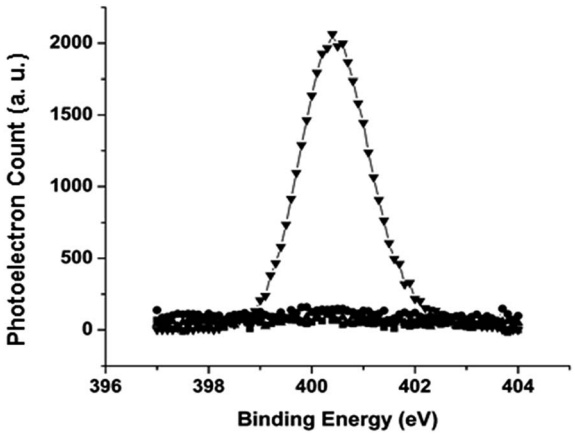

Fig. 7 High resolution N 1s spectra after the fibrinogen adsorption experiments for H–Si(111) (▼), and $C_{10}EG_7$ films on Si(111) surfaces, which were freshly-prepared (■), or maintained in ambient conditions for 14 d (●), or in PBS at 37 °C for 28 d (▲).

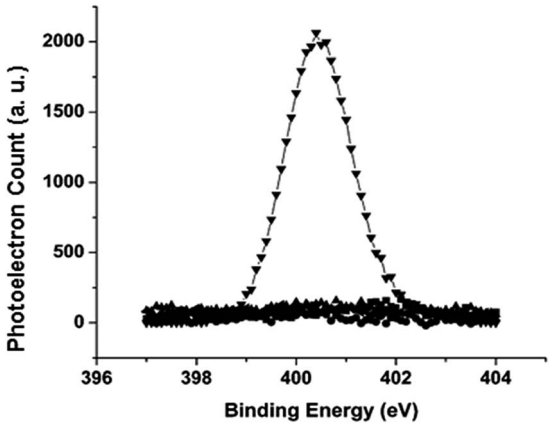

Fig. 8 High resolution N 1s spectra of a monolayer of fibrinogen on H–Si(111) (▼) and $C_{10}EG_7$ films on Si(111) in MC3T3-E1 cell culture for 17 d (■), αMEM with 10% FBS for 12 d (●), D1 cell culture for 7 d (▲) and DMEM with 10% FBS for 5 d (◂).

Conclusion

Protein-resistant films derived from a series of α-oligo(ethylene glycol)-ω-alkenes ($\mathbf{C_{m+2}EG_n}$, m = 8, 9, n = 3–7) with odd and even numbers of methylene chains (m) and various numbers of EG units (n) were prepared on H–Si(111) surfaces by photo-induced hydrosilylation under low (~1 mbar) and medium (~0.05 mbar) vacuum conditions. All films generally exhibited a low hysteresis of water contact angles, indicating a high homogeneity. Both the film thickness and resistance to protein adsorption were improved when the films were prepared at improved vacuum conditions. Under the same vacuum conditions, the even-numbered $\mathbf{C_{10}EG_n}$ films exhibit both higher thickness and better resistance to protein adsorption than the odd-numbered $\mathbf{C_{11}EG_n}$ films with the equal number of EG units. Furthermore, the films derived from $\mathbf{C_{11}EG_n}$ with $n \geq 5$ and $\mathbf{C_{10}EG_n}$ with $n \geq 4$ reduced the adsorption of fibrinogen to <3% monolayer as they were prepared at medium vacuum conditions. The optimal film $\mathbf{C_{10}EG_7}$ on Si(111) prepared at a high vacuum (10^{-5} mbar) showed no protein adsorption, and good stability in various media including cell culture media.

Acknowledgements

This work was supported by the National Science Foundation grants DMR-0706627, DMR-1207583 and DMR-1508722, the Welch Foundation grant E-1498, University of Houston (GEAR and TcSAM Special Funding), the Spanish Research Project CTQ13-48418P and CTQ16-76311, and the Marie Curie COFUND program "U-mobility" co-financed by University of Málaga and the European Community's Seventh Framework Programme under Grant Agreement No. 246550.

Notes and references

1 (*a*) A. Andres-Arroyo, B. Gupta, F. Wang, J. J. Gooding and P. J. Reece, *Nano Lett.*, 2016, **16**, 1903–1910; (*b*) X. Cheng, E. Hinde, D. M. Owen, S. B. Lowe, P. J. Reece, K. Gaus and J. J. Gooding, *Adv. Mater.*, 2015, **27**, 6144–6150.

2 (*a*) V. R. Gonçales, Y. Wu, B. Gupta, S. G. Parker, Y. Yang, S. Ciampi, R. Tilley and J. J. Gooding, *J. Phys. Chem. C*, 2016, **120**, 15941–15948; (*b*) Q. N. Minh, S. P. Pujari, B. Wang, Z. Wang, H. Haick, H. Zuilhof and C. J. M. van Rijn, *Appl. Surf. Sci.*, 2016, **387**, 1202–1210; (*c*) S. P. Pujari, E. van Andel, O. Yaffe, D. Cahen, T. Weidner, C. J. M. van Rijn and H. Zuilhof, *Langmuir*, 2013, **29**, 570–580.

Open Access Article. Published on 03 March 2017. Downloaded on 12/4/2025 11:40:37 AM.
This article is licensed under a Creative Commons Attribution 3.0 Unported Licence.

3 Y. Paska, T. Stelzner, S. Christiansen and H. Haick, *ACS Nano*, 2011, **5**, 5620–5626.
4 K. Smaali, D. Guerin, V. Passi, L. Ordronneau, A. Carella, T. Melin, E. Dubois, D. Vuillaume, J. P. Simonato and S. Lenfant, *J. Phys. Chem. C*, 2016, **120**, 11180–11191.
5 M. W. Shinwari, M. J. Deen and D. Landheer, *Microelectron. Reliab.*, 2007, **47**, 2025–2057.
6 (*a*) S. Ciampi, M. H. Choudhury, S. A. B. A. Ahmad, N. Darwish, A. Le Brun and J. J. Gooding, *Electrochim. Acta*, 2015, **186**, 216–222; (*b*) B. Fabre, Y. Li, L. Scheres, S. P. Pujari and H. Zuilhof, *Angew. Chem., Int. Ed.*, 2013, **52**, 12024–12027.
7 M. Birkholz, A. Mai, C. Wenger, C. Meliani and R. Scholz, *Wiley Interdiscip. Rev.: Nanomed. Nanobiotechnol.*, 2016, **8**, 355–377.
8 S. Kumar, V. Vandana, C. M. S. Rauthan, V. K. Kaul, S. N. Singh and P. K. Singh, *IEEE J. Photovolt.*, 2014, **4**, 380–386.
9 G. Panzarasa, G. Soliveri and V. Pifferi, *J. Mater. Chem. C*, 2016, **4**, 340–347.
10 H. Abiri, M. Abdolahad, M. Gharooni, S. A. Hosseini, M. Janmaleki, S. Azimi, M. Hosseini and S. Mohajerzadeh, *Biosens. Bioelectron.*, 2015, **68**, 577–585.
11 M. N. Masood, S. Chen, E. T. Carlen and A. van den Berg, All-(111) Surface Silicon Nanowires: Selective Functionalization for Biosensing Applications, *ACS Appl. Mater. Interfaces*, 2010, **2**, 3422–3428.
12 B. Gupta, K. Mai, S. B. Lowe, D. Wakefield, N. D. Girolamo, K. Gaus, P. J. Reece and J. J. Gooding, *Anal. Chem.*, 2015, **87**, 9946–9953.
13 (*a*) B. Guan, A. Magenau, S. Ciampi, K. Gaus, P. J. Reece and J. J. Gooding, *Bioconjugate Chem.*, 2014, **25**, 1282–1289; (*b*) Y. Zhu, A. H. Soeriyadi, S. G. Parker, P. J. Reece and J. J. Gooding, *J. Phys. Chem. B*, 2014, **2**, 3582–3588.
14 B. Guan, A. Magenau, K. A. Kilian, S. Ciampi, K. Gaus, P. J. Reece and J. J. Gooding, *Faraday Discuss.*, 2011, **149**, 301–317.
15 D. L. Sonin, D. V. Korolev, V. N. Postnov, E. B. Naumysheva, E. I. Pochkaeva, M. L. Vasyutina and M. M. Galagudza, *Drug Delivery*, 2016, **23**, 1747–1756.
16 R. E. Fernandez, V. Hareesh, E. Bhattacharya and A. Chadha, *Biosens. Bioelectron.*, 2009, **24**, 1276–1280.
17 J. Bowen and D. Cheneler, *Nanoscale*, 2016, **8**, 4245–4521.
18 M. del Rey, R. A. da Silva, D. Meneses, D. F. S. Petri, J. Tamayo, M. Calleja and P. M. Kosaka, *Sens. Actuators, B*, 2014, **204**, 602–610.
19 C. L. Kolarcik, S. D. Luebben, S. A. Sapp, J. Hanner, N. Snyder, T. D. Y. Kozai, E. Chang, J. A. Nabity, S. T. Nabity, C. F. Lagenaur and X. T. Cui, *Soft Matter*, 2015, **11**, 4847–4861.
20 L. R. Hochberg, M. D. Serruya, G. M. Friehs, J. A. Mukand, M. Saleh, A. H. Caplan, A. Branner, D. Chen, R. D. Penn and J. P. Donoghue, *Nature*, 2006, **442**, 164–171.
21 S. Kamath, D. Bhattacharyya, C. Padukudru, R. B. Timmons and L. P. Tang, *J. Biomed. Mater. Res., Part A*, 2008, **86**, 617–626.
22 J. Yakovleva, R. Davidsson, A. Lobanova, M. Bengtsson, S. Eremin, T. Laurell and J. Emneus, *Anal. Chem.*, 2002, **74**, 2994–3004.
23 M. J. Sweetman, C. J. Shearer, J. G. Shapter and N. H. Voelcker, *Langmuir*, 2011, **27**, 9497–9503.
24 J. P. Seymour and D. R. Kipke, Neural probe design for reduced tissue encapsulation in CNS, *Biomaterials*, 2007, **28**, 3594–3607.
25 M. Huebner, M. Ben Haddada, C. Methivier, R. Niessner, D. Knopp and S. Boujday, *Biosens. Bioelectron.*, 2015, **67**, 334–341.
26 R. Murthy, B. M. Bailey, C. Valentin-Rodriguez, A. Ivanisevic and M. A. Grunlan, *J. Polym. Sci., Part A: Polym. Chem.*, 2010, **48**, 4108–4119.
27 A. S. Anderson, A. M. Dattelbaum, G. A. Montano, D. N. Price, J. G. Schmidt, J. S. Martinez, W. K. Grace, K. M. Grace and B. I. Swanson, *Langmuir*, 2008, **24**, 2240–2247.
28 F. Cecchet, B. De Meersman, S. Demoustier-Champagne, B. Nysten and A. M. Jonas, *Langmuir*, 2006, **22**, 1173–1181.
29 N. Shirahata and A. Hozumi, Ultrathin poly(ethylene glycol) monolayers formed by chemical vapor deposition on silicon substrates, *J. Nanosci. Nanotechnol.*, 2006, **6**, 1695–1700.
30 S. J. Sofia, V. Premnath and E. W. Merrill, *Macromolecules*, 1998, **31**, 5059–5070.
31 R. Contreras-Caceres, C. M. Santos, S. H. Li, A. Kumar, Z. L. Zhu, S. S. Kolar, M. A. Casado-Rodriguez, Y. K. Huang, A. McDermott, J. M. López-Romero and C. Cai, *J. Colloid Interface Sci.*, 2015, **458**, 112–118.
32 M. CalistriYeh, E. J. Kramer, R. Sharma, W. Zhao, M. H. Rafailovich, J. Sokolov and J. D. Brock, *Langmuir*, 1996, **12**, 2747–2755.
33 T. Tsukagoshi, Y. Kondo and N. Yoshino, *Colloids Surf., B*, 2007, **54**, 82–87.
34 (*a*) S. C. Lange, E. van Andel, M. M. J. Smulders and H. Zuilhof, *Langmuir*, 2016, **32**, 10199–10205; (*b*) Z. Wang and H. Zuilhof, *Langmuir*, 2016, **32**, 6310–6318.
35 A. T. Nguyen, J. Baggerman, J. M. J. Paulusse, H. Zuilhof and C. J. M. van Rijn, *Langmuir*, 2012, **28**, 604–610.
36 A. T. Nguyen, J. Baggerman, J. M. J. Paulusse, C. J. M. van Rijn and H. Zuilhof, *Langmuir*, 2011, **27**, 2587–2594.
37 K. H. A. Lau, C. L. Ren, S. H. Park, I. Szleifer and P. B. Messersmith, *Langmuir*, 2012, **28**, 2288–2298.
38 L. Cao, S. Sukavaneshvar, B. D. Ratner and T. A. Horbett, *J. Biomed. Mater. Res., Part A*, 2006, **79**, 788–803.
39 J. R. Capadona, D. M. Collard and A. J. Garcia, *Langmuir*, 2003, **19**, 1847–1852.
40 C. Fairman, J. Z. Ginges, S. B. Lowe and J. J. Gooding, *ChemPhysChem*, 2013, **14**, 2183–2189.
41 S. S. Li, D. Y. Yang, H. Y. Tu, H. T. Deng, D. Du and A. D. Zhang, *J. Colloid Interface Sci.*, 2013, **402**, 284–290.
42 S. Herrwerth, W. Eck, S. Reinhardt and M. Grunze, *J. Am. Chem. Soc.*, 2003, **125**, 9359–9366.
43 S. Herrwerth, T. Rosendahl, C. Feng, J. Fick, W. Eck, M. Himmelhaus, R. Dahint and M. Grunze, *Langmuir*, 2003, **19**, 1880–1887.

 This journal is © The Royal Society of Chemistry 2017

Open Access Article. Published on 03 March 2017. Downloaded on 12/4/2025 11:40:37 AM.
This article is licensed under a Creative Commons Attribution 3.0 Unported Licence.

44 M. Rosso, A. T. Nguyen, E. de Jong, J. Baggerman, J. M. J. Paulusse, M. Giesbers, R. G. Fokkink, W. Norde, K. Schroën, C. J. M. van Rijn and H. Zuilhof, *ACS Appl. Mater. Interfaces*, 2011, **3**, 697–704.
45 L. Y. Li, S. F. Chen, J. Zheng, B. D. Ratner and S. Y. Jiang, *J. Phys. Chem. B*, 2005, **109**, 2934–2941.
46 X. F. Hu and C. B. Gorman, *Acta Biomater.*, 2014, **10**, 3497–3504.
47 M. J. Felipe, P. Dutta, R. Pernites, R. Ponnapati and R. C. Advincula, *Polymer*, 2012, **53**, 427–437.
48 B. S. Flavel, M. Jasieniak, L. Velleman, S. Ciampi, E. Luais, J. R. Peterson, H. J. Griesser, J. G. Shapter and J. J. Gooding, *Langmuir*, 2013, **29**, 8355–8562.
49 D. E. Heath, A. R. M. Sharif, C. P. Ng, M. G. Rhoads, L. G. Griffith, P. T. Hammond and M. B. Chan-Park, *Lab Chip*, 2015, **15**, 2073–2089.
50 C. M. Yam, M. Deluge, D. Tang, A. Kumar and C. Z. Cai, *J. Colloid Interface Sci.*, 2006, **296**, 118–130.
51 J. Zheng, L. Y. Li, S. F. Chen and S. Y. Jiang, *Langmuir*, 2004, **20**, 8931–8938.
52 J. Zheng, L. Y. Li, H. K. Tsao, Y. J. Sheng, S. F. Chen and S. Y. Jiang, *Biophys. J.*, 2005, **89**, 158–166.
53 K. S. Lee, I. In and S. Y. Park, *Appl. Surf. Sci.*, 2014, **313**, 532–536.
54 M. Zwahlen, S. Herrwerth, W. Eck, M. Grunze and G. Hahner, *Langmuir*, 2003, **19**, 9305–9310.
55 Y. C. Chiag, Y. Chang, W. Y. Chen and R. C. Ruaan, *Langmuir*, 2012, **28**, 1399–1407.
56 M. Rosso, A. T. Nguyen, E. de Jong, J. Baggerman, J. M. J. Paulusse, M. Giesbers, R. G. Fokkink, W. Norde, K. Schroën, C. J. M. v. Rijn and H. Zuilhof, *ACS Appl. Mater. Interfaces*, 2011, **3**, 697–704.
57 T. Hayashi, Y. Tanaka, Y. Koide, M. Tanaka and M. Hara, *Phys. Chem. Chem. Phys.*, 2012, **14**, 10196–10206.
58 G. T. Qin and C. Z. Cai, *Nanotechnology*, 2009, **20**, 355306.
59 G. T. Qin, J. H. Gu, K. Liu, Z. D. Xiao, C. M. Yam and C. Z. Cai, *Langmuir*, 2011, **27**, 6987–6994.
60 M. Sanchez-Molina, J. M. Lopez-Romero, J. Hierrezuelo-Leon, M. Martin-Rufian, M. Valpuesta and R. Contreras-Caceres, *Asian J. Org. Chem.*, 2016, **5**, 550–559.
61 A. Lucena-Serrano, C. Lucena-Serrano, R. Contreras-Caceres, A. Diaz, M. Valpuesta, C. Cai and J. M. Lopez-Romero, *Appl. Surf. Sci.*, 2016, **360**, 419–428.
62 R. J. Flamers, *Annu. Rev. Anal. Chem.*, 2008, **1**, 707–736.
63 K. A. Kilian, T. Bocking, K. Gaus, M. Gal and J. J. Gooding, *Biomaterials*, 2007, **28**, 3055–3062.
64 K. A. Kilian, T. Bocking, S. Ilyas, K. Gaus, W. Jessup, M. Gal and J. J. Gooding, *Adv. Funct. Mater.*, 2007, **17**, 2884–2890.
65 T. L. Lasseter, B. H. Clare, N. L. Abbott and R. J. Hamers, *J. Am. Chem. Soc.*, 2004, **126**, 10220–10221.
66 G. T. Qin, C. M. Santos, W. Zhang, Y. Li, A. Kumar, U. J. Erasquin, K. Liu, P. Muradov, B. W. Trautner and C. Cai, *J. Am. Chem. Soc.*, 2010, **132**, 16435–16441.
67 M. Stutzmann, J. A. Garrido, M. Eickhoff and M. S. Brandt, *Phys. Status Solidi*, 2006, **203**, 3424–3437.
68 C. M. Yam, J. H. Gu, S. Li and C. Z. Cai, Comparison of resistance to protein adsorption and stability of thin films derived from alpha-hepta-(ethylene glycol) methyl omega-undecenyl ether on H–Si(111) and H–Si(100) surfaces, *J. Colloid Interface Sci.*, 2005, **285**, 711–718.
69 C. M. Yam, J. M. Lopez-Romero, J. H. Gu and C. Z. Cai, *Chem. Commun.*, 2004, 2510–2511.
70 J. M. Buriak, *Chem. Rev.*, 2002, **102**, 1271–1308.
71 R. L. Cicero, M. R. Linford and C. E. D. Chidsey, *Langmuir*, 2000, **16**, 5688–5695.
72 Q. Y. Sun, L. de Smet, B. van Lagen, M. Giesbers, P. C. Thune, J. van Engelenburg, F. A. de Wolf, H. Zuilhof and E. J. R. Sudholter, *J. Am. Chem. Soc.*, 2005, **127**, 2514–2523.
73 J. H. Gu, C. M. Yam, S. Li and C. Z. Cai, *J. Am. Chem. Soc.*, 2004, **126**, 8098–8099.
74 G. T. Qin, R. Zhang, B. Makarenko, A. Kumar, W. Rabalais, J. M. L. Romero, R. Rico and C. Z. Cai, *Chem. Commun.*, 2010, **46**, 3289–3291.
75 E. Perez, K. Lahlil, C. Rougeau, A. Moraillon, J.-N. Chazalviel, F. Ozanam and A. C. Gouget-Laemmel, *Langmuir*, 2012, **28**, 14654–14664.
76 N. T. Flynn, T. N. T. Tran, M. J. Cima and R. Langer, *Langmuir*, 2003, **19**, 10909–10915.
77 K. Jans, K. Bonroy, R. De Palma, G. Reekmans, H. Jans, W. Laureyn, M. Smet, G. Borghs and G. Maes, *Langmuir*, 2008, **24**, 3949–3954.
78 L. Y. Li, S. F. Chen and S. Y. Jiang, *J. Biomater. Sci., Polym. Ed.*, 2007, **18**, 1415–1427.
79 Y. He, Y. Chang, J. C. Hower, J. Zheng, S. Chen and S. Jiang, *Phys. Chem. Chem. Phys.*, 2008, **10**, 5539–5544.
80 T. Hayashi, Y. Tanaka, Y. Koide, M. Tanakac and M. Hara, *Phys. Chem. Chem. Phys.*, 2012, **14**, 10196–10206.
81 A. E. Ismail, G. S. Grest and M. J. Stevens, Structure and dynamics of water near the interface with oligo(ethylene oxide) self-assembled monolayers, *Langmuir*, 2007, **23**, 8508–8514.
82 C. Fairman, J. Z. Ginges, S. B. Lowe and J. J. Gooding, *ChemPhysChem*, 2013, **14**, 2183–2189.
83 M. W. A. Skoda, R. M. J. Jacobs, J. Willis and F. Schreiber, *Langmuir*, 2007, **23**, 970–974.
84 S. Chen, L. Li, C. Zhao and J. Zheng, *Polymer*, 2010, **51**, 5283–5293.
85 G. M. Liu, Y. J. Chen, G. Z. Zhang and S. H. Yang, *Phys. Chem. Chem. Phys.*, 2007, **9**, 6073–6082.
86 L. K. Ista and G. P. Lopez, *Langmuir*, 2012, **28**, 12844–12850.
87 T. Satomi, Y. Nagasaki, H. Kobayashi, H. Otsuka and K. Kataoka, *Langmuir*, 2007, **23**, 6698–6703.
88 M. J. Shuster, A. Vaish, M. L. Gilbert, M. Martinez-Rivera, R. M. Nezarati, P. S. Weiss and A. M. Andrews, *J. Phys. Chem. C*, 2011, **115**, 24778–24787.
89 L. D. Unsworth, H. Sheardown and J. L. Brash, *Langmuir*, 2005, **21**, 1036–1041.
90 L. D. Unsworth, H. Sheardown and J. L. Brash, *Langmuir*, 2008, **24**, 1924–1929.
91 D. J. Vanderah, H. L. La, J. Naff, V. Silin and K. A. Rubinson, *J. Am. Chem. Soc.*, 2004, **126**, 13639–13641.

Open Access Article. Published on 03 March 2017. Downloaded on 12/4/2025 11:40:37 AM.
This article is licensed under a Creative Commons Attribution 3.0 Unported Licence.

92 N. Bonnet, D. O'Hagan and G. Hahner, *Phys. Chem. Chem. Phys.*, 2010, **12**, 4367–4374.
93 X. Y. Zhu, Y. Jun, D. R. Staarup, R. C. Major, S. Danielson, V. Boiadjiev, W. L. Gladfelter, B. C. Bunker and A. Guo, *Langmuir*, 2001, **17**, 7798–7803.
94 A. B. Sieval, B. van den Hout, H. Zuilhof and E. J. R. Sudholter, *Langmuir*, 2000, **16**, 2987–2990.
95 A. B. Sieval, B. van den Hout, H. Zuilhof and E. J. R. Sudholter, *Langmuir*, 2001, **17**, 2172–2181.
96 P. Gorostiza, C. H. de Villeneuve, Q. Y. Sun, F. Sanz, X. Wallart, R. Boukherroub and P. Allongue, *J. Phys. Chem. B*, 2006, **110**, 5576–5585.
97 M. F. Juarez, F. A. Soria, E. M. Patrito and P. Paredes-Olivera, *J. Phys. Chem. C*, 2008, **112**, 14867–14877.
98 L. J. Webb, D. J. Michalak, J. S. Biteen, B. S. Brunschwig, A. S. Y. Chan, D. W. Knapp, H. M. Meyer, E. J. Nemanick, M. C. Traub and N. S. Lewis, *J. Phys. Chem. B*, 2006, **110**, 23450–23459.
99 C. M. Dekeyser, C. C. Buron, K. Mc Evoy, C. C. Dupont-Gillain, J. Marchand-Brynaert, A. M. Jonas and P. G. Rouxhet, *J. Colloid Interface Sci.*, 2008, **324**, 118–126.
100 E. J. Nemanick, P. T. Hurley, B. S. Brunschwig and N. S. Lewis, *J. Phys. Chem. B*, 2006, **110**, 14800–14808.
101 L. E. O'Leary, E. Johansson, B. S. Brunschwig and N. S. Lewis, *J. Phys. Chem. B*, 2010, **114**, 14298–14302.
102 C. Hogan, L. Caramella and G. Onida, *Phys. Status Solidi B*, 2012, **249**, 1132–1139.
103 C. M. Yam, J. Gu, S. Li and C. Cai, *J. Colloid Interface Sci.*, 2005, **285**, 711–718.
104 A. Ulman, *An Introduction to Ultrathin Organic Films: From Langmuir–Blodgett to Self-Assembly*, Academic Press, Boston, 1991.
105 D. Briggs and M. P. Seah, *Practical Surface Analysis by Auger and X-ray Photoelectron Spectroscopy*, Wiley, New York, 1984.
106 M. James, T. A. Darwish, S. Ciampi, S. O. Sylvester, Z. Zhang, A. Ng, J. J. Gooding and T. L. Hanley, *Soft Matter*, 2011, **7**, 5309–5318.
107 C. Wang, H. Lu, Z. Wang, P. Xiu, B. Zhou, G. Zuo, R. Wan, J. Hu and H. Fang, *Phys. Rev. Lett.*, 2009, **103**, 137801.
108 C. Wang, B. Zhou, P. Xiu and H. Fang, *J. Phys. Chem. C*, 2011, **115**, 3018–3024.
109 T. Ye, E. A. McArthur and E. Borgue, *J. Phys. Chem. B*, 2005, **109**, 9927–9938.
110 T. Ye, D. Wynn, R. Dudek and E. Borguet, *Langmuir*, 2001, **17**, 4497–4500.
111 F. Tao and S. L. Bernasek, *Chem. Rev.*, 2007, **107**, 1408–1453.
112 J. C. Love, L. A. Estroff, J. K. Kriebel, R. G. Nuzzo and G. M. Whitesides, *Chem. Rev.*, 2005, **105**, 1103–1169.

 This journal is © The Royal Society of Chemistry 2017